CONNECTING SYMMETRIC AND ASYMMETRIC FAMILIES OF PERIODIC ORBITS IN SQUARED SYMMETRIC HAMILTONIAN

FERNANDO BLESA

Departamento de Física Aplicada
Universidad de Zaragoza, E-50009 Zaragoza, Spain
fblesa@unizar.es

SLAWOMIR PIASECKI

Departamento de Matemática Aplicada
Universidad de Zaragoza, E-50009 Zaragoza, Spain
piasek@unizar.es

ÁNGELES DENA

Centro Universitario de la Defensa
Academia General Militar, E-50090 Zaragoza, Spain
adena@unizar.es

ROBERTO BARRIO

Departamento de Matemática Aplicada and IUMA
Universidad de Zaragoza, E-50009 Zaragoza, Spain
rbarrio@unizar.es

In this work, we study a generic squared symmetric Hamiltonian of two degrees of freedom. Our aim is to show a global methodology to analyze the evolution of the families of periodic orbits and their bifurcations. To achieve it, we use several numerical techniques such as a systematic grid search algorithm in sequential and parallel, a fast chaos indicator and a tool for the continuation of periodic orbits. Using them, we are able to study the special and generic bifurcations of multiplicity one that allow us to understand the dynamics of the system and we show in detail the evolution of some symmetric breaking periodic orbits.

Keywords: Periodic orbits; symmetric Hamiltonians; bifurcations of periodic orbits.

1. Introduction

The study of Hamiltonian systems of two-degrees of freedom has been done by a large number of researchers by using different techniques. Nowadays, it is possible to mix several of these methods in order to provide a more complete study of the systems. Besides, most of the techniques can be extended to systems with more degrees of freedom. The main purpose of this paper is to focus on this global approach, that is, to use several methods, most of them already used by other authors and adapted to the current computational tools like parallel computing, in order to study a particular important problem that has not been analyzed completely in the literature.

When we want to study a Hamiltonian system, one of the most common ways to proceed is to perform several Poincaré Surfaces of Section to determine how the system evolves as the energy changes. In this paper, we propose to combine that study with more specific techniques such as a chaotic indicator and a search of symmetric periodic orbits to have a better vision of the invariants of the system, with the goal to understand the dynamics in a greater detail. One of these invariant objects are the families of periodic orbits.

The importance of studying periodic orbits in nonintegrable Hamiltonian systems with two degrees of freedom has been recognized since Poincaré,[1] as it is a route to understand the nonintegrable dynamics of the system. The periodic orbits can be thought as the skeleton of the dynamics.[2,3] In particular, if the periodic orbits are symmetric, they can be computed using a grid search method.[4–8] As the flow is continuous, a trajectory near a periodic orbit will present a similar dynamics. Therefore, the knowledge of the families of periodic orbits of a system and their stability will give us a better understanding of the phase space structure.[9]

The periodic orbits play an important role in several physical applications, such as in chaotic billiards,[10] in the control of chaotic dynamical systems,[11] in the plasma physics,[12] in the transition state theory of chemical reactions,[13] in the studies of the scars in a quantum system[14,15] or in celestial mechanics and mission design,[16,17] among other applications.

In this paper, we are going to analyze a Hamiltonian system with a quartic potential that posses square symmetries using some numerical tools. We are going to show the complex structure of its phase space and to study the progressive loss of symmetry in the periodic orbits after each bifurcation until we obtain a family of asymmetric periodic orbits.

This paper is organized as follows. In Sec. 2, we explain the generic quartic Hamiltonian, in Sec. 3 we describe the numerical techniques that we have used to analyze this problem. In Sec. 4, we show the evolution of the system as the energy grows, in Sec. 5, we study the main bifurcations of multiplicity one of systems with symmetry D_4, in Sec. 6 we compute some asymmetric families that appear in this problem and we show their evolution and finally, in Sec. 7 we show how to decrease the computing time of the systematic grid search method by parallelizing the algorithm.

2. The Quartic Hamiltonian

An interesting generic family of Hamiltonian system is given by $\mathcal{H} = \frac{1}{2} \times (\dot{x}^2 + \dot{y}^2) + V(x, y)$ with the quartic potential

$$V(x, y) = \frac{1}{2} n(x^2 + y^2) + \alpha x^2 y^2 + \frac{1}{4} \beta (x^4 + y^4), \tag{1}$$

that was proposed by Andrle[18] for a stellar system with an axis and a plane of symmetry, and later used in many applications. This potential depends on parameters $n, \alpha, \beta \in \mathbb{R}$, and it is known to be integrable for some values of the parameters.[19–21] If we take $n > 0$, then it can be considered to model two coupled isotropic oscillators that has been analyzed in problems related to quantum chaos[21,22] and galactic dynamics.[23,24] If however $n < 0$, it can be considered as a model for two coupled Duffing oscillators.[18]

This Hamiltonian presents the D_4 symmetry, that is, it is invariant under a rotation by $\pi/2$. It has also the time-reversal symmetry.

This model has been studied previously for several values of the parameters. Without being exhaustive, some interesting examples are the following:

- The Yang–Mills potential[25] ($n = 0, \alpha = 1, \beta = 0$), first thought to be completely ergodic, but later known to posses stable periodic orbits[26]

$$V(x, y) = x^2 y^2.$$

- The galactic potential[27,28] ($n = 1, \alpha = -1, \beta = 0$) with four escapes, that has been object of studies by some authors, and it has been observed to posses safe regular regions[29] for energies above the escape energy

$$V(x, y) = \frac{1}{2}(x^2 + y^2) - x^2 y^2.$$

- The homogeneous quartic oscillator[17,19,30–33] ($n = 0, \alpha = 1, \beta = 1$), that has been studied from a classical, semiclassical and quantum-mechanical perspective

$$V(x, y) = \frac{1}{4}(x^4 + y^4) + x^2 y^2.$$

- The dihedral potential[34] ($n = -2, \alpha = 1/4, \beta = 1$) (see Fig. 1)

$$V(x, y) = \frac{1}{4}(x^2 + y^2)^2 - (x^2 + y^2) - \frac{1}{4} x^2 y^2. \tag{2}$$

In this paper, we are going to analyze the dihedral potential (Eq. (2)). It has been previously considered by some authors[35,36] in the context of galactical dynamics, where they analyzed their mixing properties. This Hamiltonian also appears[34] when studying the Bogdanov−Takens bifurcation at the origin. This bifurcation has interest in fluid dynamics related to convection problems in a container such as in a magnetoconvention[37,38] model with a vertical magnetic field, but it can also

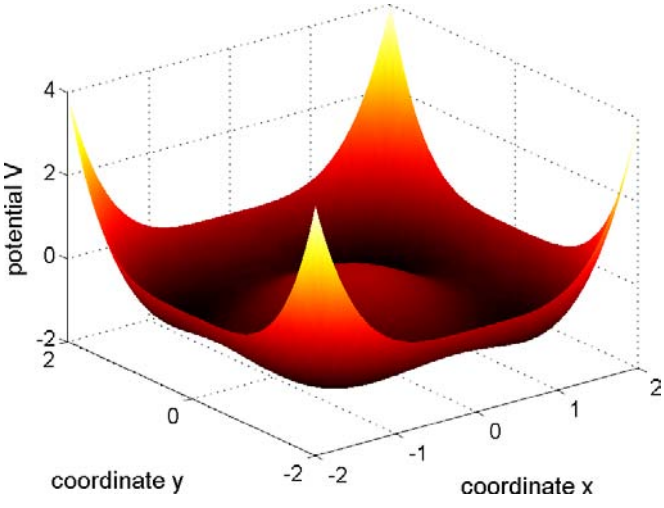

Fig. 1. (Color online) Dihedral potential (Eq. (2)).

appear in models with a salt gradient (thermohaline convection), a Coriolis force or other stabilizing effects (see Ref. 37 for more details). Due to this stabilizing vertical gradient, the otherwise $O(2)$ symmetry of the convection problem is broken and a D_4 symmetric system (assuming a square container; other symmetries are possible in other containers) remains that depends on a parameter. The variation of this parameter allows to study the Bogdanov−Takens codimension two bifurcation on those systems. In a limit case the system is Hamiltonian[34] with the potential of Eq. (2).

Note that, the bifurcations found in this system may appear in any D_4 symmetric system, and so this analysis is general.

3. Numerical Techniques

In this section, we describe briefly the numerical techniques used to study the dynamics of the Hamiltonian system, namely, to compute its Poincaré surfaces of section, to find the chaotic regions, to perform a systematic search of symmetric periodic orbits and to continue families of periodic orbits.

One of the most common tools used to analyze dynamical systems is the Poincaré Surface of Section (PSS). The basic idea is to select a 2D manifold transverse to most of the trajectories of the system and to study their cuts. In our case, the manifold has to be chosen to be transverse to all orbits.[39]

Another interesting thing is to locate the chaotic regions. One of the tools useful for that goal is a chaos indicator, that is a fast numerical technique used to detect chaos. Two common chaos indicators, based on variational methods, are the Fast Lyapunov Indicator[40,41] (FLI) and the Orthogonal Fast Lyapunov Indicator[41] (OFLI).

The OFLI2[42] method adds to FLI and OFLI the use of the second order variational equations to minimize the appearance of spurious structures.[43] Therefore, the OFLI2 indicator at the final time t_f is given by

$$\text{OFLI2} := \sup_{t_0<t<t_f} \log \left\| \{\boldsymbol{\xi}(t) + \frac{1}{2}\delta\boldsymbol{\xi}(t)\}^{\perp} \right\|, \tag{3}$$

where $\boldsymbol{\xi}$ and $\delta\boldsymbol{\xi}$ are the first and second order sensitivities with respect to carefully chosen initial vectors and $\boldsymbol{g}^{\perp}$ denotes the component of $\boldsymbol{g}$ orthogonal to the flow. In this case, the variational equations up to second order and the initial conditions are given by

$$\begin{aligned}
&\frac{d\boldsymbol{\rho}}{dt} = \boldsymbol{f}(t,\boldsymbol{\rho}), && \boldsymbol{\rho}(t_0) = \boldsymbol{\rho}_0,\\
&\frac{d\boldsymbol{\xi}}{dt} = \frac{\partial \boldsymbol{f}(t,\boldsymbol{\rho})}{\partial \boldsymbol{\rho}}\boldsymbol{\xi}, && \boldsymbol{\xi}(t_0) = \frac{\boldsymbol{f}(t_0,\boldsymbol{\rho}_0)}{\|\boldsymbol{f}(t_0,\boldsymbol{\rho}_0)\|},\\
&\frac{d\delta\xi_j}{dt} = \frac{\partial f_j}{\partial \boldsymbol{\rho}}\delta\boldsymbol{\xi} + \boldsymbol{\xi}^{\top}\frac{\partial^2 f_j}{\partial \boldsymbol{\rho}^2}\boldsymbol{\xi}, && \delta\boldsymbol{\xi}(t_0) = \mathbf{0}.
\end{aligned} \tag{4}$$

Note that, the last line of Eq. (4) is written for a single j-th component $\delta\xi_j$ to simplify the notation.

OFLI2 tends to a constant value for the periodic orbits, behaves as $\log t$ for initial conditions on a KAM tori and on a regular resonant motion but with different rate of growing (and so they grow linearly in a logarithmic time scale as in Fig. 2) and grows exponentially for chaotics orbits.

In Fig. 2, we show the evolution of the OFLI2 values in the time interval $[1, 10^4]$ for four particular orbits of the Hénon−Heiles problem. The orbits are indicated with the letters −a− (a periodic orbit), −b− and −c− (orbits on a KAM tori) and −d− (a chaotic orbit).

From now on, in the figures with the OFLI2 results, we have used the red color to point the chaotic regions and blue for the most regular ones, being the intermediate colors the transition from one to the other situation.

To compute the symmetric periodic orbits, we use (see Ref. 44 for more details of our implementation) a method based on the classical systematic search method.

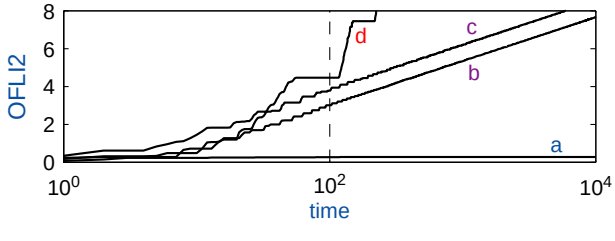

Fig. 2. (Color online) Evolution of the OFLI2 values in the time interval $[1, 10^4]$ for four particular orbits: −a− (a periodic orbit), −b− and −c− (orbits on a KAM tori) and −d− (a chaotic orbit).

This method is easily parallelizable, and in Sec. 7 we show some tests that we have carried out. This method, for two degrees of freedom Hamiltonians with some symmetries, was used to obtain the skeleton of symmetric periodic orbits shown in Fig. 3(a). The procedure to obtain the skeleton contains several steps. First, the Poincaré map is computed in a particular well-chosen plane. It is important to include the symmetry conditions into the section for the systematic search. Plane $(x, \dot{x})$ was choosen with $y = 0$, and $\dot{y}$ was obtained from the energy. With these conditions the Poincaré sections are symmetric or reversing symmetric with respect to x-axis. Now, if a solution is $\{x(t), y(t)\}$ and depends on system symmetries, then $\{x(-t), -y(t)\}$ or $\{x(t), -y(t)\}$ is also a solution. Let us consider an orbit which starts at a position perpendicular to the x-axis

$$(x(0), y(0), \dot{x}(0), \dot{y}(0)) = (x_0, 0, 0, \dot{y_0}), \tag{5}$$

and crosses the x-axis again perpendicularly, then the orbit is closed and symmetric. This happens exactly at half period of the orbit. Therefore, next step is to check the

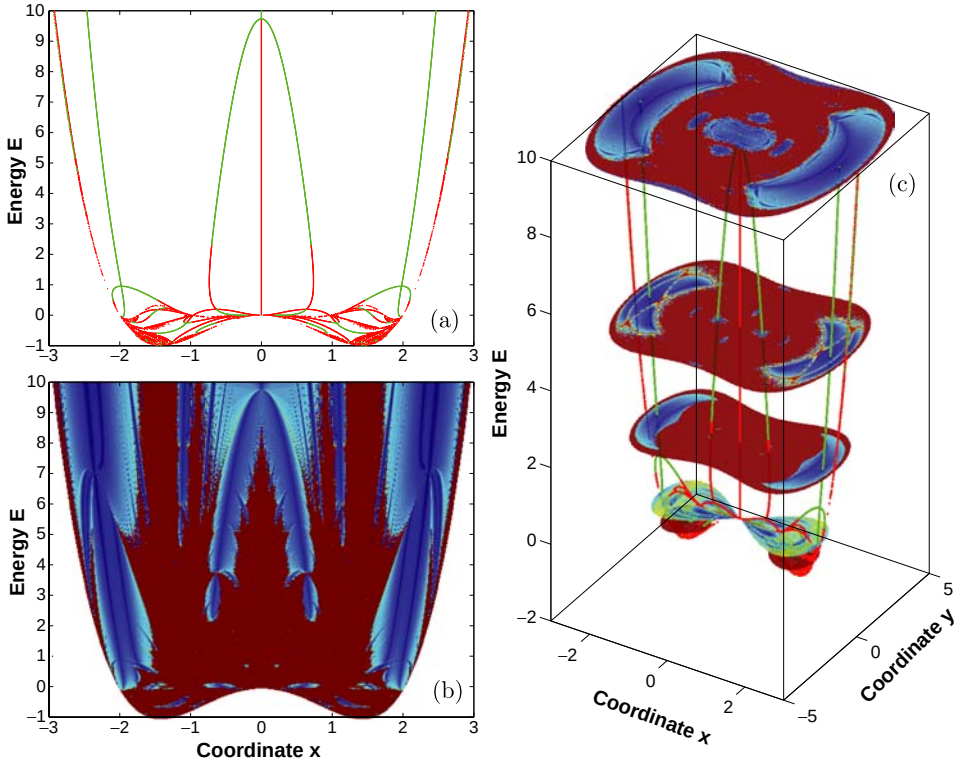

Fig. 3. (Color online) (a) Skeleton of symmetric periodic orbits of multiplicity $m = 1$. Green represents stable and red unstable symmetric periodic orbits. (b) OFLI2 chaos indicator. Red corresponds to the chaotic region and blue to the stable region. (c) Combined OFLI2 (x, y) plots for different values $\{0.5, 0.0, 2.0, 5.0, 10.0\}$ of the energy together with the skeleton of symmetric periodic orbits.

existence of a symmetric periodic orbit at half period $T/2$ of the orbit with the following condition

$$y(x_0, 0, 0, \dot{y_0}(0); T/2) = \dot{x}(x_0, 0, 0, \dot{y_0}; T/2) = 0. \tag{6}$$

For other kind of symmetries the conditions are similar and therefore the same or a similar method may be used. In particular, in our Hamiltonian system, we could also have chosen the plane $(y, \dot{y})$ due to the D_4 symmetry.

In order to proceed with the search of periodic orbits the first step is to give a mesh $N \times N$ in the parameter and variable space. As our system is an autonomous Hamiltonian system with two degrees of freedom, the Hamiltonian is an integral of motion. Thus, we use the energy $E \equiv \mathcal{H}$ as a parameter and we perform a mesh in the plane (x, E). Each pair gives a complete set of initial conditions. Then, we integrate until we find the chosen Poincaré Surface of Section after a number of crossings of the x-axis with $\dot{y} > 0$ equal to the multiplicity of the orbit we are looking for. After this we need to combine the integration of the orbit with a rootfinding process to obtain an orbit with $\dot{x} = 0$ that will be a symmetric periodic orbit.

With the systematic search method we are only able to obtain families of symmetric periodic orbits, so we have to use another method for the asymmetric families of periodic orbits. Therefore, our last method is the continuation of families of periodic orbits. We use the AUTO software package which is based on the continuation theory for ODEs.[45]

AUTO uses the pseudo-arclength continuation method. As an initial condition we choose a periodic orbit that is perturbed on the energy parameter. As explained in Ref. 46 we need to formulate our problem as a boundary value problem introducing an unfolding term with an unfolding parameter. The solution is another periodic orbit with a new energy value in a predictor−corrector algorithm. The computations are repeated for new initial conditions, and so we get a complete family and its bifurcations.

4. Evolution of the D_4 Symmetric System

One interesting problem when studying dynamical systems is to analyze the evolution of the system when one parameter is changed. In this section, we use the numerical techniques explained in the previous section to obtain the skeleton of periodic orbits and a classification of regions according to its chaotic or regular behavior.

Figure 3 shows the evolution of the system as the energy grows. Inset (a) presents the skeleton of symmetric periodic orbits of multiplicity $m = 1$. We can see that, there are many families just of this multiplicity. In green color, we plot the stable periodic orbits and in red the unstable ones. In plate (b) the result of the OFLI2 chaos indicator is presented. The colors that appear on this plot are blue and red, as mentioned above, and they correspond to regular and chaotic regions, respectively. Comparing the two plots, we can see how the results of both techniques match

perfectly one each other, but we have to take into account that the OFLI2 method collects information about all the orbits, and not only those of multiplicity $m = 1$.

A more complete evolution of the families of periodic orbits is presented at Fig. 3(c), where we have combined the previously explained skeleton of periodic orbits together with several OFLI2 plots for some values of the energy. This plot shows not only the periodic orbits, but also the KAM tori around the periodic orbits and the chaotic regions. We can see how the system evolves as the energy grows. For very low values of the energy ($E = -0.5$), the system appears to be very chaotic and is divided in two disconnected regions. When the energy increases to $E = 0.0$, the two regions touch and are connected at $x = 0$. In the OFLI2 plots, we can see several complex structures with islands due to periodic orbits (blue), separated by chaotic regions (red). If we further increase the energy, we see at $E = 2.0$, $E = 5.0$ and $E = 10.0$, that the two regions are now completely connected and new structures appear and merge. As observed, there is a correspondence with the skeleton of periodic orbits. At $E = 5.0$, new structures appear that evolve as the energy grows, and at $E = 10.0$, those islands have merged into a bigger structure. A similar evolution happens around the edges, where some families appear, giving rise to some new islands.

These plots show us how the system evolves when the energy changes, but to complement this study we have to analyze the bifurcations of the system.

5. Bifurcations on the System

We are interested in studying the behavior of the system in the vicinity of a periodic orbit. Therefore, we want to calculate the stability of the orbit. As it is known, the eigenvalues of the monodromy matrix $\Pi_1 := \Pi(T)$ allow us to study the linear stability of the periodic orbit. The monodromy matrix is the solution at time T (the period of the periodic orbit) of the first order variational equations

$$\dot{\Pi} = \mathcal{J} \cdot \mathrm{Hess}(\mathcal{H}(\boldsymbol{q}, \boldsymbol{p})) \cdot \Pi, \quad \text{with } \Pi(0) = I_4, \tag{7}$$

where $\mathcal{J}$ is the canonical symplectic matrix , I_4 the 4D identity matrix, and Hess $(\mathcal{H}(\boldsymbol{u}))$ the Hessian matrix of $\mathcal{H}$ with respect of $\boldsymbol{u}$. In the particular case of Hamiltonians of the form $\mathcal{H}(\boldsymbol{q}, \boldsymbol{p}) = \frac{1}{2}(\boldsymbol{p} \cdot \boldsymbol{p}) + U(\boldsymbol{q})$, such as ours, the variational equations take the simple form

$$\dot{\Pi} = \begin{pmatrix} 0 & I_2 \\ -\mathrm{Hess}(U(\boldsymbol{q})) & 0 \end{pmatrix} \Pi, \quad \text{with } \Pi(0) = I_4. \tag{8}$$

Since the system (2) is a Hamiltonian system, the monodromy matrix Π_1 is a real symplectic matrix and we have that its eigenvalues $\{\lambda_i, i = 1, \ldots, 4\}$ are in reciprocal pairs

$$\lambda_1 \lambda_2 = 1, \quad \lambda_3 \lambda_4 = 1.$$

The complex eigenvalues are also in complex conjugate pairs. In order to study the stability of orbits, the stability index κ is defined as follows[47]

$$\kappa = \kappa(\Pi(T)) := \mathrm{Tr}(\Pi(T)) - 2. \tag{9}$$

It is always possible to write the stability index in this form because there is always an eigenvalue equal to one for a periodic orbit and therefore its reciprocal is also equal to one. Thus, just the λ_3 and λ_4 eigenvalues remain to study. As they are complex conjugate (when complex) and reciprocal they are on the unit circle in the complex plane or on the real axis. In case when both eigenvalues are on the unit circle $|\kappa| < 2$, and the studied periodic orbit is stable. Unstable case occurs when λ_3 and λ_4 are real ($|\kappa| > 2$). If the eigenvalues are equal to one or minus one ($|\kappa| = 2$), a special case appears, it is the point where the stability may change.

The isochronous bifurcation point in the family of periodic orbits appears when $\kappa = \lambda_3 + \lambda_4 = 2\mathrm{Re}(\lambda_{3,4}) = 2$. This allows us to know when such a bifurcation occurs.

5.1. *Bifurcations of multiplicity* $m = 1$

In this section, we describe the "typical"[48] local bifurcations of the families of periodic orbits for systems with squared symmetry. This means that different bifurcations may happen, but they would be exceptional.

We are going to study with some detail the symmetric bifurcations of multiplicity $m = 1$. Other typical bifurcations may happen for higher multiplicities.

In Fig. 4, we show a scheme of a Poincaré section of the typical bifurcations of our system, taking into account that the Poincaré section may appear rotated. We suppose that the bifurcation happens when the parameter has the value $\mathcal{P}_B$ and we write $\mathcal{P} = \mathcal{P}_B + \varepsilon$. We show just one direction, from $\varepsilon < 0$ to $\varepsilon > 0$, but the bifurcation may occur in the opposite direction. The bifurcation B1 is generic,[48] that is, it may appear on systems having symmetries or not. After a family of periodic orbits has lost all its symmetries, this is the only typical bifurcation of multiplicity one. For systems with the D_4 symmetry, there are other possible bifurcations B2, B3, B4 and B5, but they involve a loss of some symmetries in the new families of periodic orbits.

The case B1 corresponds to a saddle-node bifurcation. For this bifurcation, two periodic orbits are created one being stable and the other one unstable (we mark the unstable orbits with a red cross in Fig. 4). This is the only way of creating new families of periodic orbits (apart from the boundaries of the domain of definition of the Hamiltonian system).

The bifurcations B2 and B3 are symmetric pitchfork and antipitchfork: two new periodic orbits are created from a symmetric periodic orbit but they loss symmetries. The new orbits are isochronous with the main periodic orbit (i.e. they have multiplicity one as well) and they are stable (B2) or unstable (B3). The main symmetric orbit changes its stability.

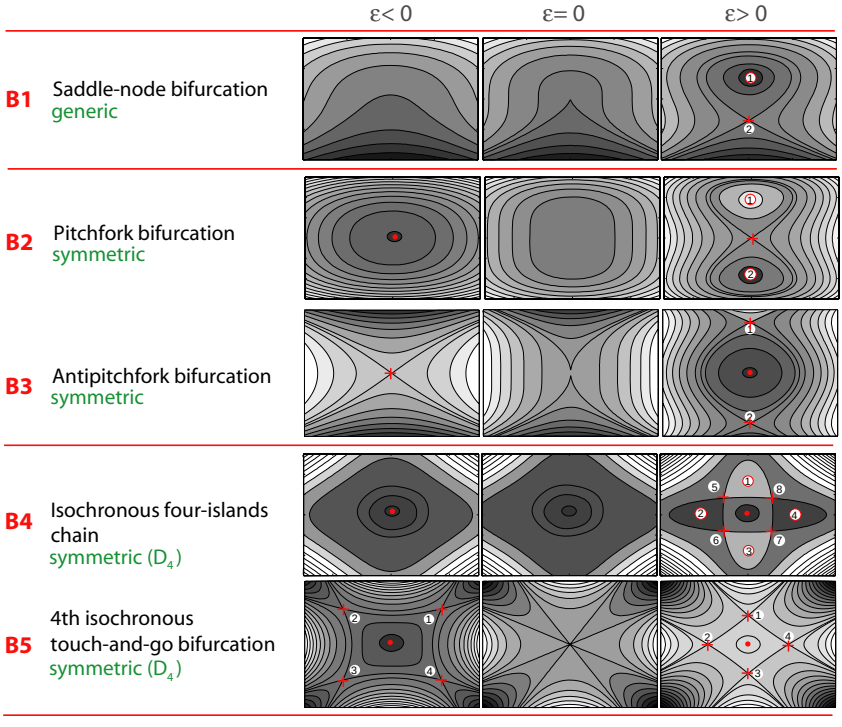

Fig. 4. (Color online) Generic and special bifurcations of local multiplicity $m = 1$ in a D_4 symmetric Hamiltonian system.

The case B4 corresponds to the creation of resonance islands of local multiplicity $m = 1$ around the main orbit that remains stable. The orbits on the islands lose their D_4 symmetry.

Finally, the case B5 is another special bifurcation (called touch-and-go), where four unstable periodic orbits (without D_4 symmetry) of local multiplicity one touch the center orbit that is symmetric and stable and "bounce" after a rotation.

As already mentioned, the system that is studied in this paper has the D_4 symmetry, so we can find these bifurcations in it. We illustrate some of these bifurcations in our problem on the plots of Figs. 5 and 6, by showing an OFLI2 plot and a PSS for values of the energy before ($\varepsilon < 0$) and after ($\varepsilon > 0$) the bifurcations.

In Fig. 5, we show when the B3 antipitchfork bifurcation occurs in our system. For an energy before the bifurcation ($E = 0.25$) there is only an unstable periodic orbit. After the bifurcation ($E = 0.12$) the unstable orbit becomes stable and in the right plot there is a zoom of the bifurcated stable family. Note that the bifurcation appears as the energy decreases, so the sign of ε changes.

In Fig. 6, we show the B4 four-islands chain of multiplicity one bifurcation. Before the bifurcation ($E = 1.30$), there is just one stable orbit, and after it ($E = 0.85$), there is a chain of four-islands with four new stable orbits at the

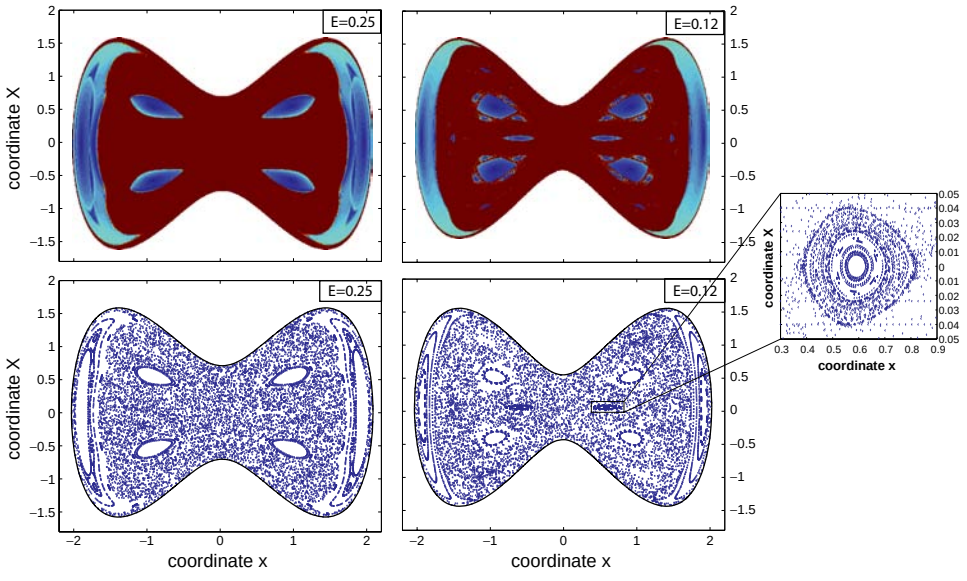

Fig. 5. (Color online) OFLI2 (top) and Poincaré surface of section (bottom) before (left $E = 0.25$) and after (right $E = 0.12$) bifurcation (antipitchfork) on plane $(x, \dot{x})$. On the right, magnification of the bifurcated stable family.

center and another four unstable orbits connecting the islands. The D_4 symmetry of each individual orbit is lost, but all together keep the symmetry of the system. These periodic orbits for a particular value of the energy are plotted in Fig. 8(c).

Note that, Fig. 4 is presented here just to illustrate some of the bifurcations of our problem, without doing a complete study of Hamiltonian bifurcations under symmetries which is out of the scope of the present paper (see the extensive literature on this subject[48−52] for a more detailed explanation).

The normal forms[53] of these bifurcations of multiplicity $m = 1$, are presented in Table 1. In particular, the normal form for the B4 bifurcation is[53]

$$f_\epsilon(\rho, \theta) = \frac{1}{2}\varepsilon\rho^2 + \frac{1}{4}a\rho^4 + \frac{1}{4}b\rho^4\cos(4\phi) + \cdots \tag{10}$$

where a, b are constants and $(\rho,\ \phi)$ are polar coordinates. If ε is positive and passes through zero to a negative value, then the origin becomes a maximum (for $|a| > |b|$). At the bifurcation point, four stable and unstable families symmetrically placed appear, and this situation is called a "four-islands chain" bifurcation. The normal form of the four-islands chain of isochronous bifurcation (B4) is plotted in Fig. 4, and at this case four stable and four unstable periodic orbits are created and the main family remains stable.

If $|a| < |b|$ we get the B5 touch-and-go bifurcation. In this system, we have not been able to observe this bifurcation for orbits of local multiplicity $m = 1$.

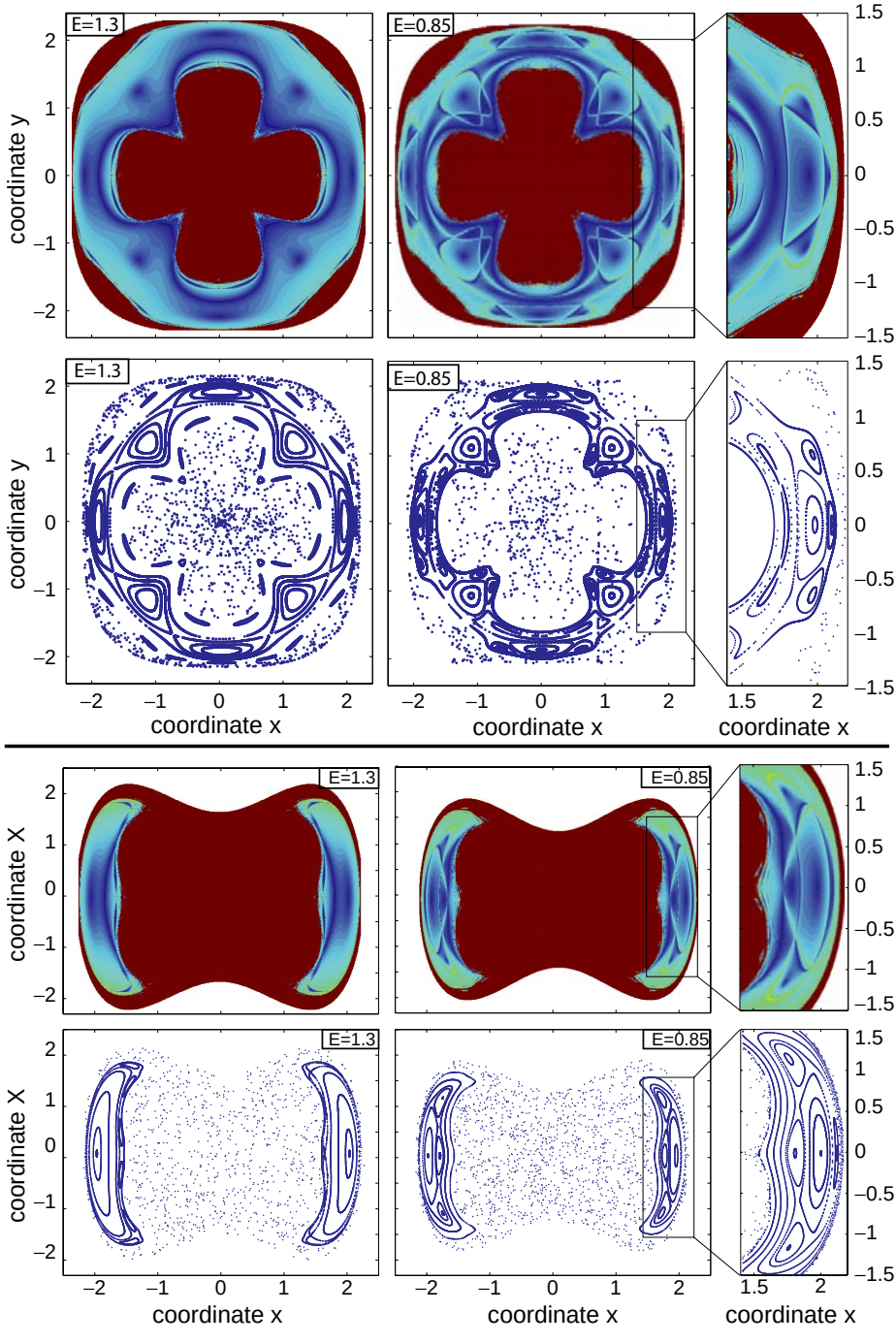

Fig. 6. (Color online) OFLI2 (top) and Poincaré surface of section (bottom) on both (x, y) and $(x, \dot{x})$ planes before (left $E = 1.30$) and after (middle $E = 0.85$) bifurcation (special bifurcation four-islands chain) point on plane $(x, \dot{x})$. On the right magnification of the bifurcated family, for $E = 0.85$.

Table 1. Normal forms of the bifurcations of multiplicity $m = 1$ of Fig. 4.

Bifurcation	Normal form	
B1	$f_\epsilon(q,p) = \frac{1}{2}p^2 + \frac{1}{3}q^3 + \varepsilon q$	
B2	$f_\epsilon(q,p) = \frac{1}{2}bp^2 + \frac{1}{4}aq^4 + \frac{1}{2}\varepsilon q^2$	$ab < 0$
B3		$ab > 0$
B4	$f_\epsilon(\rho,\theta) = \frac{1}{4}a\rho^4 + \frac{1}{4}b\rho^4\cos(4\phi) + \frac{1}{2}\varepsilon\rho^2$	$\lvert a\rvert > \lvert b\rvert$
B5		$\lvert a\rvert < \lvert b\rvert$

In Fig. 7, we show the evolution of the stability index of the main (blue) and the bifurcated (green) families at the four-islands bifurcation. When the main family has a stability index $\kappa = 2$, the bifurcated family appears. Inset (a) shows a (E, κ) plot, whereas (b) shows (x, κ). The main family appears at a saddle-node bifurcation at a negative energy value. The stable branch undergoes a period doubling bifurcation

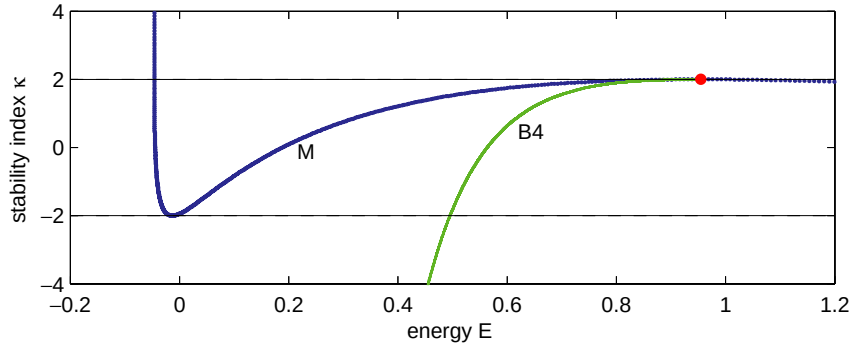

(a)

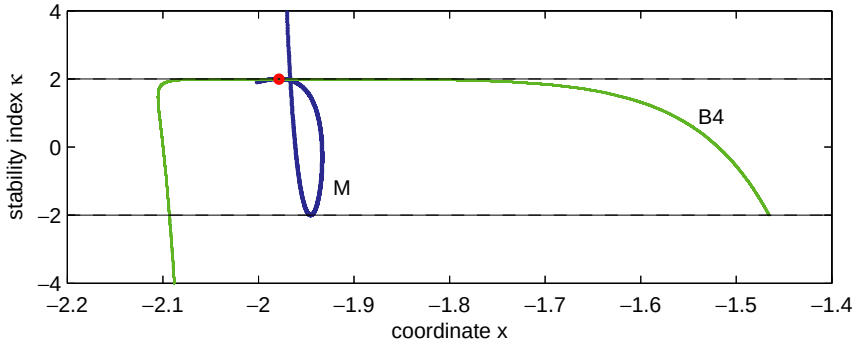

(b)

Fig. 7. (Color online) (a) Stability index versus energy and (b) stability index versus coordinate x, for two families at the four-islands chain of isochronous bifurcation. Blue color represents the main family $\{M\}$ while green corresponds to the bifurcated family $\{\mathrm{B4}\}$.

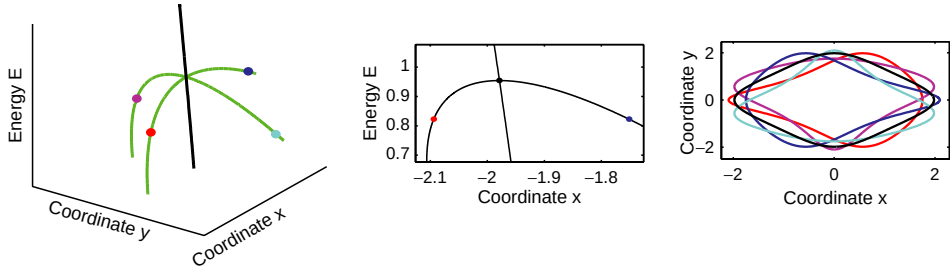

(a) (b) (c)

Fig. 8. (Color online) (a) Outline of the stable orbits of the four-islands chain isochronous bifurcation on plane (x, y) versus Energy and (c) selected orbits. (b) shows the skeleton obtained from AUTO. In black we plot the main family and in the other colors the four stable bifurcated families.

slighly below $E = 0$, and then the energy grows until it reaches the isochronous four-islands bifurcation near $E = 1$, shown as a red dot. Note that the family of periodic orbits is still stable after the bifurcation, as the stability index bounces back at 2. The bifurcated families appear as a single curve in (a). Nevertheless, in (b) we see that in fact the families present different values of the coordinate x and we are able to separate them. The other two stable families can be separated plotting the coordinate y and the four unstable families are rotated.

To have the whole picture of the bifurcated families, we show in Fig. 8 the schematic representation of the four-islands chain (B4) bifurcation diagram. In panel (a) we have the evolution of the four stable families versus the Energy. In (b), we show just the skeleton of periodic orbits as usually computed and in (c), we plot the four periodic orbits for a value of the energy (shown as a colored dot at the center and left plots). In (c), each color corresponds to an orbit. Note that, on black we have the main symmetric periodic orbit. The other colors correspond to the stable bifurcated periodic orbits. Each of them has lost the D_4 symmetry, but they still have other symmetries.

6. Connecting Symmetric and Asymmetric Families of Periodic Orbits in Symmetric Hamiltonians

We have so far computed symmetric periodic orbits using our systematic search method, but this system also presents families of periodic orbits without symmetries. To obtain them, we are going to use the AUTO[45] software that, as mentioned previously, uses a continuation method. With AUTO, it is possible to obtain families of periodic solutions, starting from a known periodic orbit and continuing it. At the same time, AUTO can locate the bifurcations, and continue the bifurcated families at the bifurcation points. These points are the starting points for the next computations, where new families of periodic orbits are detected and are characterized by dropping one symmetry.

Figure 9 shows several families of periodic orbits with their bifurcation points. There is a family that performs a whole loop while it undergoes several bifurcations as the energy changes, as shown in the stability index plot in Fig. 9 (right-bottom). We are going to describe this figure as we move through these bifurcations. Since the figure is symmetric, we are going to consider positive values of the coordinate x because the same bifurcations will happen for negative values of x. At the saddle-node bifurcation point BP1 ($x = 0.149, E = -7.5 \times 10^{-5}$), two orbits are created. The unstable family ends at the stable point at $x = 0$. The stable family increases the value of the coordinate x until it arrives at the antipitchfork bifurcation BP2 ($x = 0.636, E = 0.193$) where it becomes unstable. At the same time, two unstable families are created. One of them finishes at the stable point $x = 0$. The other finishes at ($x = 0.96, E = 0$). Their stability index is shown in Fig. 9 (right). Continuing with the main family, it presents a pitchfork bifurcation at BP3 ($x = 0.702, E = 2.3$). At this point, two stable asymmetric families appear and quickly become unstable through a period doubling bifurcation, ending again at the stable point $x = 0$. Their stability index is shown in Fig. 9 (right). Finally, the main family finishes at the bifurcation point BP4 ($x = 0, E = 9.73$), which is a pitchfork bifurcation of the vertical family $\{a\}$ that is born at the stable point $x = 0$. That family becomes stable as seen in the stability index plot and keeps its stable character even for big values of the energy.

Note that, the curve corresponding to the linear family exists for all positive values of the Energy exactly at $x = 0$. This family has just the reflexion symmetry in

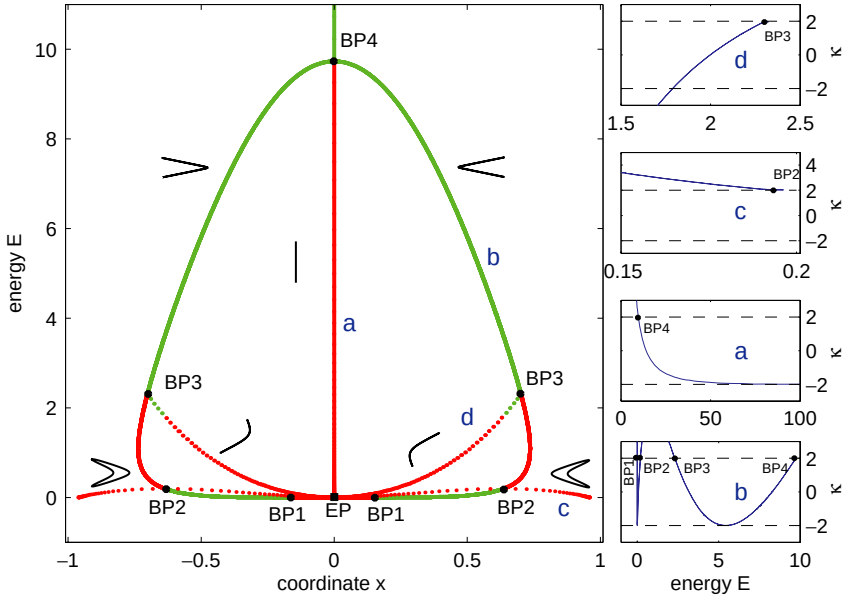

Fig. 9. (Color online) Symmetric and asymmetric families of periodic orbits. On right panels we show the stability index κ for these families. Green color denotes stable periodic orbits and red color unstable periodic orbits.

both x and y axis. The other families bifurcate from it, so neither of those families present the D_4 symmetry, and they lose one symmetry after each bifurcation. At BP4, the x-axis reflexion symmetry is lost, and then, either at BP3 the y-axis reflexion symmetry is lost or at BP2 the time-reversal symmetry is lost.

In Fig. 9 (right), there are four panels that correspond to the stability index κ versus the energy E of the main orbit (bottom), of the $\{a\}$ family, and the two bifurcated families from the main loop family. As we can see, the $\{c\}$ family is always unstable whereas the $\{d\}$ family is initially stable until it undergoes a period doubling bifurcation and remains unstable until it collides at the origin.

In Fig. 10, we show with more detail the evolution of the symmetric periodic orbits (with reflexion symmetry) of the main loop family $\{b\}$. On panel (b), we plot the whole family. In green, we show the stable periodic orbits and in red the unstable ones. The blue dots in panel (b) indicate the orbits projected into the (x, y) plane in panel (c), where we see that the orbits evolve from an orbit deformed to the right to the vertical orbit as it goes through BP4, and then in reverse direction to an orbit to the left. In panel (a), we show a 3D plot with the orbits in the $(x, y, \dot{x})$ variables.

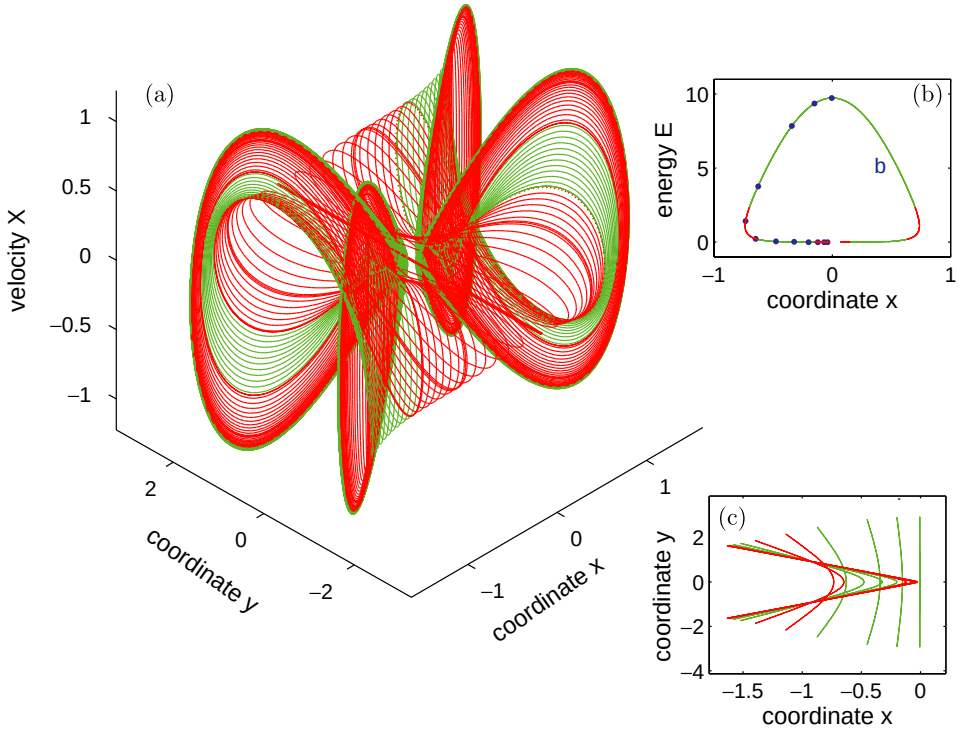

Fig. 10. (Color online) (a) Evolution of symmetric periodic orbits of the loop family $\{b\}$ of Fig. 9. Panel (b) plot presents the main family. Panel (c) shows the evolution of the orbits on the plane (x, y). Red color corresponds to unstable periodic orbits and green color to stable periodic orbits.

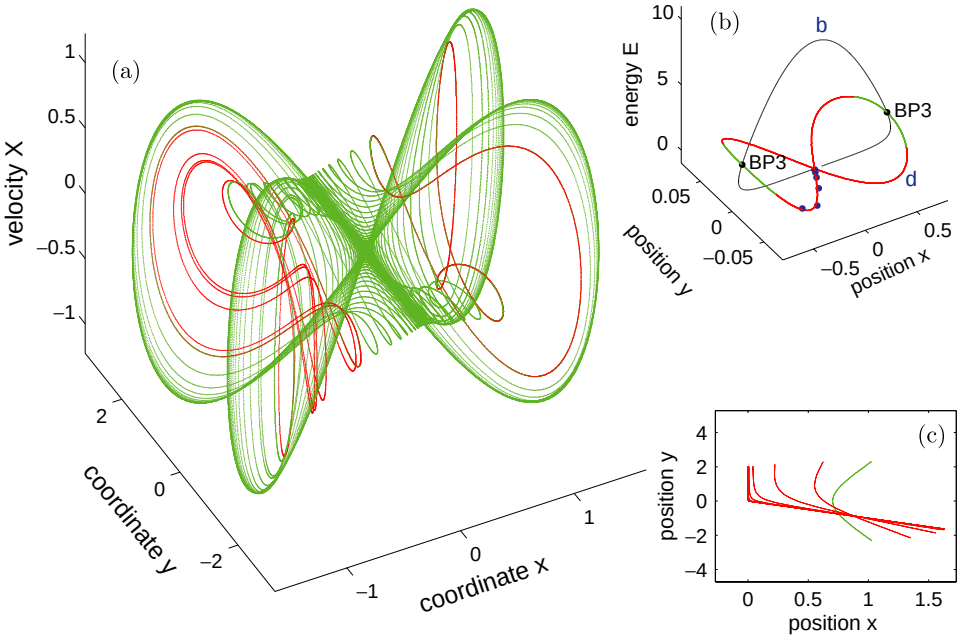

Fig. 11. (Color online) (a) Evolution of asymmetric periodic orbits of the family $\{d\}$ of Fig. 9. Panel (b) presents on black the main symmetric family $\{b\}$, whereas the asymmetric family $\{d\}$ is represented in red color the unstable orbits and in green the stable ones. Panel (c) shows the evolution of the orbits on the plane (x, y).

We see that, the unstable orbits move through more space volume although most of the family is stable as seen in (b).

In Fig. 11, we present the evolution of some asymmetric periodic orbits. On panel (b), we show the asymmetric family $\{d\}$. In black, we plot the main family that is shown in detail in Fig. 10. Again green and red orbits are the stable and unstable periodic orbits of the family. At each BP3 bifurcation points, two families of periodic orbits appear to preserve the reflexion symmetry of the main loop family as already seen in Fig. 9. One of the orbits moves to the forward direction and the other one to the backward direction. To show this on panel (b), we present them in a 3D plot where in the horizontal plane we plot the value of the x coordinate at the PSS. The blue dots are some selected orbits that are shown in (c), where we can see the evolution of the orbits in the (x, y) plane and their lack of symmetry. The family rotates to an almost horizontal orbit when the family arrives at the origin. Finally on panel (a) we have a 3D plot with the evolution of the orbits in the $(x, y, \dot{x})$ variables.

7. High Order Multiplicities and Parallel Study of the Problem

In this section, we describe an improvement of the systematic grid search method, namely the parallelization of the code in order to decrease the computing time.

When we compute, not only periodic orbits of multiplicity one but also of higher order multiplicities, we approach to the approximate general solution of the problem[54] by means of computing a dense set of families of periodic orbit that allow us to describe globally the behavior of the Hamiltonian system.

In Fig. 12, we show the symmetric periodic orbits in the plane (x, E) of multiplicities $m = 2$, 4 and 6. Last figure shows all the multiplicities from 1 to 6. In Table 2, we present the number of the orbits found and classified by its multiplicity that span from $m = 1$ to 12. We have repeated this test for a grid of 500×500 points, computing thousands of orbits and another grid of 1000×1000 points, obtaining about seven hundred thousand orbits. We see here that, as expected, the complexity increases with the multiplicity and so the computing time will be greater.

The computer time increases with the multiplicity, so the use of multiple cores of modern computers can give us an important boost, decreasing the time needed to finish the computation. In our case, the systematic grid search method is an easily

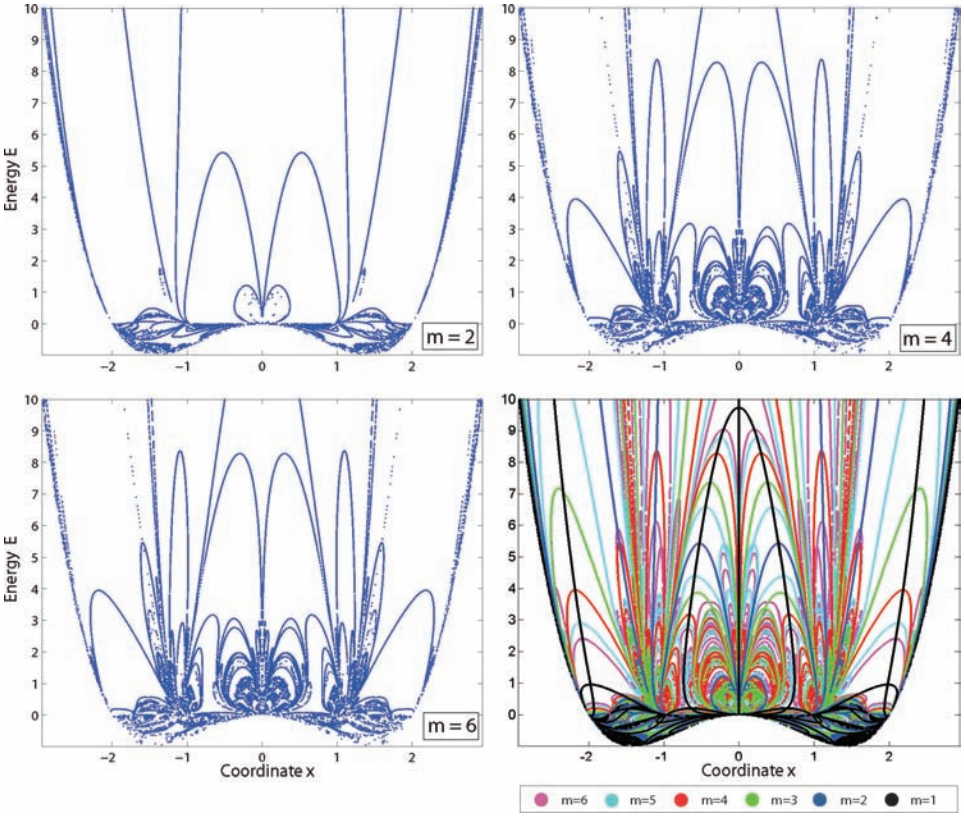

Table 2. Number of orbits computed with multiplicities that span from 1 to 12, for grids 500×500 and 1000×1000.

500×500	$m = 1$	2	3	4	5	6	
Num. of orbits	3,682	5,866	14,035	19,152	23,618	21,369	
500×500	7	8	9	10	11	12	Total
Num. of orbits	20,322	16,071	14,315	10,940	10,641	8,306	168,317
1000×1000	$m = 1$	2	3	4	5	6	
Num. of orbits	9,041	16,022	42,002	65,411	92,296	95,846	
1000×1000	7	8	9	10	11	12	Total
Num. of orbits	96,919	84,756	78,625	64,127	59,057	48,777	752,879

parallelizable algorithm, as it is divisible into parts and it can be directly used with OpenMP or MPI.

The grid search algorithm studies consecutively each of the N horizontal lines and next each of the N vertical lines (grid $N \times N$). In each line, we use the information of two consecutive points to calculate the zero. We remark that no information of the previous lines is needed. Therefore, we parallelize the algorithm simply by computing each line on each processor.

In this work, we have used a personal computer PC Intel quad-core i7, CPU 860, 2.80 GHz under a 2.6.32-29-generic SMP x86 64 Linux system and the supercomputer HECToR (High End Computing Terascale Resources) that is located at the University of Edinburgh in Scotland. HECToR's hardware configuration (2011, phase 2b (XE6)) contains a large number of compute nodes, each one with two 12-core AMD Opteron 2.1 GHz Magny Cours processors. Each 12-core processor shares 16 Gb of memory, giving a system total of 59.4 Tb. We use in this simulations one of such compute nodes.

One standard metric to measure the performance of a parallel algorithm is just the CPU-time. In Table 3, we show the CPU-time with HECToR in a grid of 500×500 points and up to multiplicity $m = 6$, depending on the number of cores. Another standard metric to measure the performance of a parallel algorithm is the *Efficiency*, $E(p)$, defined as

$$E(p) = \frac{T(1)}{p \cdot T(p)},$$

where $T(1)$ is the CPU-time (in seconds) of the sequential algorithm and $T(p)$ is the CPU-time of the parallel algorithm executed on p processors. In the benchmarking

Table 3. CPU-time (seconds) and efficiency on HECToR for each number of cores in a grid 500×500 up to multiplicity $m = 6$.

Cores	$p = 1$	2	4	8	12	16	20	24
CPU	4717.	2363.	1235.	627.2	420.3	318.3	260.5	218.7
$E(p)$	—	0.998	0.954	0.940	0.935	0.926	0.905	0.899

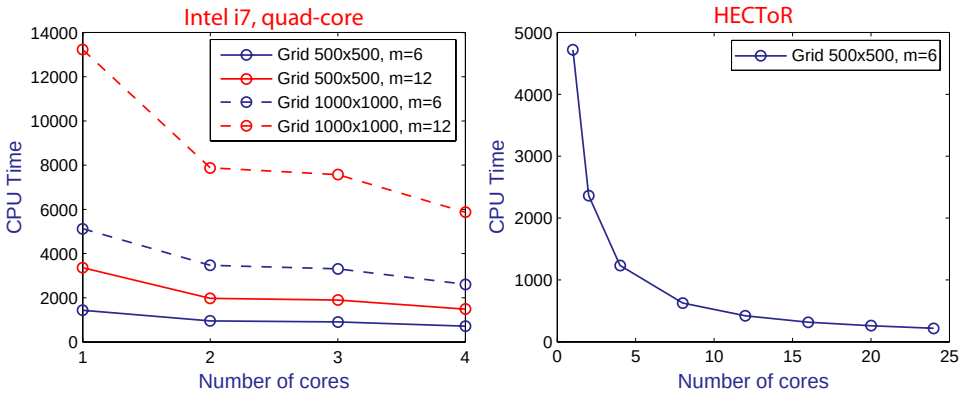

Fig. 13. (Color online) CPU-time versus number of cores. On the left, with an Intel i7 quad-core computer and on the right, with HECToR.

test, we have obtained very good results and a relative efficiency around 90% with 24 cores of HECToR computer.

Nowadays, the personal computers are multicore (dual-core, quad-core, six-core), so it is interesting and useful to use the power provided to us by these modern computers. As it is shown in Fig. 13, the CPU-time is similar using the same number of cores with an usual computer or with a supercomputer like HECToR although it has thousands cores. On the left, we can see the CPU-time on a quad-core Intel i7 computer showing that the complete use of a modern multicore processor permits to reduce significatively the global time of computing. On the right, we observe that using more and more cores on HECToR, the algorithm will permit to perform very detailed studies in a reasonable time.

8. Conclusion

In this paper, we show the generic structure of D_4 Hamiltonian symmetric systems via the detailed study of a particular case of interest. To perform our analysis, we have used several numerical methods to study the dynamics of such systems. This kind of systems appears frequently in different fields like in galactic dynamics, quantum and semiclassical chaos, coupled classical oscillators, and some others. The results obtained with the study of this particular case can be directly extended to these problems.

We study the evolution of the different families via systematic search methods in the symmetric case and continuation methods for the asymmetric case. The study is complemented with a careful analysis of the chaotic and regular regions of the system using the OFLI2 chaos indicator, which joined with the skeleton of periodic orbits gives a detail study of the dynamics of the system. Different bifurcations of periodic orbits, both generic and special (taking into account the symmetries of the

system), are also presented. All these bifurcations and generic dynamics are presented in most of the D_4 symmetric systems.

Finally, we show that we can decrease significatively the computing time for some of our computation, by using a parallel code together with the power of a modern multicore computer.

Acknowledgments

The authors F.B. and S.P. acknowledge support from the Spanish Research project AYA2008-05572 and R.B and A.D. from the Spanish Research project MTM2009-10767. The work of A.D. was carried out under the HPC-EUROPA2 project (project number: 228398) with the support of the European Commission - Capacities Area - Research Infrastructures. Besides, this work made use of the facilities of HECToR, the UK's national high-performance computing service, which is provided by UoE HPCx Ltd at the University of Edinburgh, Cray Inc and NAG Ltd, and funded by the Office of Science and Technology through EPSRC's High End Computing Programme.

References

1. H. Poincaré, *Les méthodes nouvelles de la mécanique céleste*, Vol. 1−3, (Gauthier-Villars et fils, 1892−1899).
2. G. D. Birkhoff, *Rend Circ Mat Palermo* **39**, 334 (1915).
3. E. Strömgren, *Bull. Astron.* **9**, 87 (1925).
4. R. DeVogelaere, *Contributions to the Theory of Nonlinear Oscillations*, Vol. 4 (Princenton University Press, 1958), pp. 53−84.
5. M. Hénon, *Ann. Astrophys.* **28**, 992 (1965).
6. M. N. Vrahatis, *J. Comput. Phys.* **119**, 105 (1995).
7. V. V. Markellos, W. Black and P. E. Moran, *Celest. Mech. Dyn. Astron.* **9**, 507 (1974).
8. G. Tsirogiannis, E. Perdios and V. V. Markellos *Celest. Mech. Dyn. Astron.* **103**, 49 (2008).
9. P. Cvitanović and B. Eckhardt, *Phys. Rev. Lett.* **63**, 823 (1989).
10. A. D. Stone, *Nature* **465**, 696 (2010).
11. E. Ott, C. Grebogi and J. A. Yorke, *Phys. Rev. Lett.* **64**, 1196 (1990).
12. E. C. da Silva, I. L. Caldas, R. L. Viana and M. A. F. Sanjuán, *Phys. Plasmas* **9**, 4917 (2002).
13. T. Uzer, C. Jaffé, J. Palacián, P. Yanguas and S. Wiggins, *Nonlinearity* **15**, 957 (2002).
14. E. J. Heller, *Phys. Rev. Lett.* **53**, 1515 (1984).
15. G. de Polavieja, F. Borondo and R. Benito, *Phys. Rev. Lett.* **73**, 1613 (1994).
16. W. S. Koon, M. W. Lo, J. E. Marsden and S. D. Ross, *Chaos* **53**, 427 (2000).
17. J. E. Marsden and S. D. Ross, *Bull. Amer. Math. Soc.* **43**, 43 (2006).
18. P. Andrle, *Bull. Astron. Inst. Czech.* **17**, 169 (1966).
19. T. Bountis, F. Segur and F. Vivaldi, *Phys. Rev. A* **25**, 1257 (1982).
20. A. Lesfari, *Arch. Math.* **77**, 347 (2001).
21. S. Ferrer, M. J. Marco, C. Osácar and J. F. Palacián, *Phys. Lett. A* **146**, 411 (1990).
22. P. A. Vorobyev and G. M. Zaslavsky, *Sov. Phys. JETP* **65**, 877 (1987).
23. N. Caranicolas and H. Varvoglis, *Astron. Astrophys.* **141**, 383 (1984).

24. A. Deprit and A. Elipe, *Celest. Mech. Dyn. Astron.* **51**, 227 (1991).
25. S. G. Matinyan, G. K. Savvidi and N. G. Ter-Arutyunyan-Savvidi, *Sov. Phys. JETP* **53**, 421 (1981).
26. P. Dahlqvist and G. Russberg, *Phys. Rev. Lett.* **65**, 2837 (1990)
27. G. Contopoulos, *Astron. Astrophys.* **231**, 41 (1990).
28. B. Barbanis, *Celest. Mech. Dyn. Astron.* **48**, 57 (1990).
29. R. Barrio, F. Blesa and S. Serrano, *New J. Phys.* **11**, 053004 (2009).
30. R. Rajaraman and E. J. Weinberg, *Phys. Rev. D* **11**, 2950 (1975).
31. M. Brack, S. N. Fedotkin, A. G. Magner and M. Mehta, *J. Phys. A* **36**, 1095 (2003).
32. H. Yoshida, *Physica A* **288**, 424 (2000).
33. S. P. Kasperczuk, *Int. J. Bifur. Chaos* **20**, 1 (2010).
34. D. Armbruster, J. Guckenheimer and S. Kim, *Phys. Lett. A* **140**, 416 (1989).
35. H. E. Kandrup, *Mon. Not. R. Astron. Soc.* **301**, 960 (1998).
36. I. Pogorelov and H. Kandrup, *Phys. Rev. E* **60**, 1567 (1999).
37. A. M. Rucklidge, *Phys. Lett. A* **284**, 99 (2001).
38. M. R. E. Proctor and N. O. Weiss, *Rep. Prog. Phys.* **45**, 1317 (1982).
39. H. R. Dullin and A. Wittek, *J. Phys. A* **24**, 7157 (1995).
40. C. Froeschlé and E. Lega, *Celest. Mech. Dyn. Astron.* **78**, 167 (2003).
41. M. Fouchard, E. Lega, C. Froeschlé and C. Froeschlé, *Celest. Mech. Dyn. Astron.* **83**, 205 (2003).
42. R. Barrio, *Int. J. Bifur. Chaos Appl. Sci. Eng.* **10**, 2777 (2006).
43. R. Barrio, W. Borczyk and S. Breiter, *Chaos Solitons Fractals* **40**, 1697 (2009).
44. R. Barrio and F. Blesa, *Chaos Solitons Fractals* **41**, 560 (2009).
45. E. J. Doedel, R. C. Paffenroth, A. R. Champneys, T. F. Fairgrieve, Y. A. Kuznetsov, B. Sandstede, B. Oldeman, X. Wang and C. Zhang, *AUTO 07P: Continuation and bifurcation software for ordinary differential equations* (2007).
46. F. J. Muñoz-Almaraz, E. Freire, J. Galán, E. Doedel and A. Vanderbauwhede, *Physica D* **181**, 1 (2003).
47. M. Hénon, *Astron. Astrophys.* **1**, 223 (1969).
48. K. R. Meyer, *Trans. Amer. Math. Soc.* **149**, 95 (1970).
49. J. M. Mao and J. B. Delos, *Phys. Rev. A* **45**, 1746 (1992).
50. M. A. M. de Aguiar, C. P. Malta, M. Baranger and K. T. R. Davies, *Ann. Phys.* **180**, 167 (1987).
51. M. A. M. de Aguiar and C. P. Malta, *Phys. D* **30**, 413 (1988).
52. P. L. Buono, F. Laurent-Polz and J. Montaldi, *London Math. Soc. Lect. Note Ser.* **306**, (Cambridge University Press, 2005), pp. 357−402.
53. D. A. Sadovskiĭ and J. B. Delos, *Phys. Rev. E* **54**, 2033 (1996).
54. K. E. Papadakis, G. A. Katsiaris and C. L. Goudas, *Astrophys. Space Sci.* **300**, 297 (2005).